Journal of Molecular and Cellular Cardiology Plus 5 (2023) 100044

Contents lists available at ScienceDirect

Journal of Molecular and Cellular Cardiology Plus

journal homepage: www.journals.elsevier.com/journal-of-molecular-andcellular-cardiology-plus

Autonomic neuro-cardiac profile of electrical, structural and neuronal remodeling in myocardial infarction-induced heart failure

Shui Hao Chin [a,b,1], Emily Allen [a,1], Kieran E. Brack [a], G. André Ng [a,b,c,*]

[a] Cardiology group, Department of Cardiovascular Sciences, University of Leicester, UK
[b] University Hospitals of Leicester NHS Trust, Leicester, UK
[c] NIHR Leicester Cardiovascular Biomedical Research Unit, Leicester, UK

ARTICLE INFO

Keywords:
Autonomic
Ganglia
Ventricular fibrillation
Restitution
Heart failure
Remodeling

ABSTRACT

Aims: Heart failure is a clinical syndrome typified by abnormal autonomic tone, impaired ventricular function, and increased arrhythmic vulnerability. This study aims to examine electrophysiological, structural and neuronal remodeling following myocardial infarction in a rabbit heart failure model to establish its neuro-cardiac profile.
Methods and results: Weight-matched adult male New Zealand White rabbits (3.2 ± 0.1 kg, $n = 25$) were randomized to have coronary ligation surgeries (HF group, $n = 13$) or sham procedures (SHM group, $n = 12$). Transthoracic echocardiography was performed six weeks post-operatively. On week 8, dual-innervated Langendorff-perfused heart preparations were set up for terminal experiments. Seventeen hearts (HF group, $n = 10$) underwent ex-vivo cardiac MRI. Twenty-two hearts (HF group, $n = 7$) were examined histologically. Electrical remodeling and abnormal autonomic profile were evident in HF rabbits with exaggerated sympathetic and attenuated vagal effect on ventricular fibrillation threshold, ventricular refractoriness and restitution curves, in addition to increased spatial restitution dispersion. Histologically, there was significant neuronal enlargement at the heart hila and conus arteriosus in HF. Structural remodeling was characterized by quantifiable myocardial scarring, enlarged left ventricles, altered ventricular geometry and impaired contractility.
Conclusion: In an infarct-induced rabbit heart failure model, extensive structural, neuronal and electrophysiological remodeling in conjunction with abnormal autonomic profile provide substrates for ventricular arrhythmias.

1. Introduction

Abnormal autonomic tone characterized by sympathetic overactivation and parasympathetic attenuation modulates malignant arrhythmogenesis in heart failure with reduced ejection fraction. As phenotyping of heart failure becomes increasingly sophisticated encompassing heart failure with reduced or preserved ejection fraction, heart failure with reduced ejection fraction will simply be referred to as 'heart failure' (HF) in this study. Preclinical [1] and clinical [2] studies have demonstrated causal link between heart rate variability and baroreceptor reflex sensitivity with fatal ventricular arrhythmias, suggesting a tentative link between impaired neuro-cardiac control and arrhythmic propensity.

The presence of a rich network of intrinsic cardiac nerves converging into distinct ganglia, has been established in humans and other mammalian species [3]. These ganglia are capable of functioning both independently of and in concert with higher neural centres, enabling the regulation of cardiac indices on a beat-to-beat basis [4]. In HF, anatomical and functional remodeling of these ganglionic plexi have been observed within this intrinsic cardiac nervous system (ICNS) [5].

In this study, we sought to establish a reproducible infarct-induced rabbit HF model that allows for histopathological, in vivo and ex vivo assessments of structural remodeling in addition to in vitro electrophysiological characterization through isolated, Langendorff-perfused hearts with intact dual autonomic nerves.

2. Methods

2.1. Ethical statement

All procedures conform to the UK Animals (Scientific Procedures)

* Corresponding author at: Department of Cardiovascular Sciences, Cardiology group, University of Leicester, Glenfield Hospital, Leicester LE39QP, UK.
E-mail address: gan1@le.ac.uk (G.A. Ng).
[1] SHC and EA contributed equally to this study

https://doi.org/10.1016/j.jmccpl.2023.100044
Received 22 November 2022; Received in revised form 25 July 2023; Accepted 16 August 2023
Available online 22 August 2023

Act 1985, *Guide for the Care and Use of Laboratory Animals* published by the US National Institutes of Health (NIH Publication No. 85-23, revised 1985) and the European Union directive on the protection of animals for scientific research (2010/63/EU). Local ethics approval was obtained from the University of Leicester animal welfare review board (AWERB) under the Home Office Project License PPL70/8501.

2.2. Rabbit myocardial infarction heart failure model (Cohort 1)

Adult male New Zealand White rabbits in Cohort 1 (3.2 ± 0.1 kg, $n = 25$) were randomly assigned to two groups: a coronary-ligation group (HF, $n = 13$); and a sham group (SHM, $n = 12$)(Supplementary Fig. 1). Male rabbits were used to allow comparison of study findings of diseased model with historical normal-heart studies within our group. Additionally, the use of male rabbits circumvents the confounding effects of estrous cyclicity on homogeneity of study population, data spread and autonomic interventions [6]. Rabbits were premedicated (Medetomidine Hydrochloride 0.2 mg/kg, Ketamine 10 mg/kg), Butorphanol Torbugesic, 0.05 mg/kg, intubated and ventilated using a Harvard small animal ventilator (tidal volume 30 ml, respiratory rate 55/min) and anaesthetized with 1–1.5 % isofluorane. Following left thoracotomy, circumflex artery was ligated midway between the atrio-ventricular groove and the apex resulting in apical discoloration consistent with a 30–40 % left ventricular infarct. No coronary ligation was performed for the SHM group. Animals were left to recover for 8 weeks before being sacrificed.

2.3. The innervated isolated heart preparation

The innervated isolated Langendorff-perfused heart preparation has previously been described [8]. Briefly, adult male New Zealand White rabbits were premedicated with a subcutaneous injection containing a mixture of Medetomidine Hydrochloride (Sedator, 0.2 mg/kg), Ketamine (Narketan, 10 mg/kg) and Butorphanol Tartrate (Torbugesic, 0.05 mg/kg). Once the animal was suitably sedated, surgery was performed to isolate rabbit heart with intact dual autonomic innervation as described in detail in previous studies. The animal was sacrificed with an overdose of intravenous pentobarbitone sodium (60 mg) and heparin (500 U). Of note, pentobarbitone sodium was chosen due to its inert effect on autonomic function not only in rabbits but other animal models [8–10]. A 3F polypropylene catheter (Portex, Kent, UK) was inserted through the left ventricular apex for Thebesian venous effluent drainage. Left ventricular pressure (LVP) was measured by a pressure transducer (MTL0380, AD Instruments, Chalgrove, UK) using a fluid-filled latex balloon inserted through the left atrium into the left ventricle (LV). The volume of the balloon was adjusted to give a 0 – 5 mmHg end-diastolic pressure reading. Perfusion pressure (PP) was monitored with a separate pressure transducer.

2.4. Autonomic nerve stimulation

The cervical vagus nerves were stimulated using a pair of custom-made bipolar silver electrodes (VNS) (Advent Research Materials, UK: 0.5 mm diameter). Bilateral sympathetic nerve stimulation (SNS) was achieved by insertion of a quadripolar catheter into the spinal canal at the 12th thoracic vertebra to the level of stellate ganglia. Stimulation was delivered using 2-channel constant voltage square pulse stimulators, (S88, Grass Instruments), one for VNS and one for SNS at 2 ms pulse width. Intercostal-muscle twitching was prevented with a neuromuscular blocking agent (decamethonium bromide [Sigma, UK, 5 μM]).

Autonomic nerves were stimulated at varying strength (1-10 V) and heart rate (HR) response recorded. The stimulus strength that produced a heart rate equivalent to 80 % of the maximal response was used throughout. SNS was carried out at a frequency giving rise to an SNS-induced tachycardia of 230–250 bpm. VNS frequency was determined as the frequency resulting in a bradycardia of 60–70 bpm. The calibration protocol based on HR response was previously described, and allowed an unbiased comparison of ventricular electrophysiology between diseased and non-diseased Langendorff-perfused rabbit hearts in this study [8].

2.5. Cardiac electrical recording and pacing

A pair of platinum electrodes (Grass Instruments, Slough, UK) were connected to the right atrial appendage for recording of atrial electrograms and a second pair to the right atrium and rib cage to record ECG. Electrodes were placed at the epicardial surface of basal and apical LV free wall for recording of monophasic action potential (MAP) using a DC-coupled high-input impedance differential amplifier. Optimal basal and apical locations for the electrode placements were determined by the quality of the MAP. In HF group, the non-scarring apex can be identified by the normal coloration of the apex to avoid the apical infarct area with poor/no signal quality for MAP acquisition. A bipolar pacing electrode was inserted into the right ventricular (RV) apex for ventricular pacing.

2.6. Measurement of ventricular electrophysiology

Functional responses were recorded with a PowerLab800.s (ADInstruments Ltd., UK) and digitalised at 2 kHz using LabChart Pro software (ADInstruments Ltd., UK). HR was recorded at steady state at baseline and following autonomic stimulation.

Ventricular fibrillation threshold (VFT) was measured with RV burst pacing (30 stimuli, 30 ms interval) after a 20-beat drivetrain at 240 ms, and was determined by progressively increasing the pacing current at 0.5 mA steps with a 5-s rest period before each drive train. VFT was defined as the minimum current required to induce sustained VF.

Standard restitution and ventricular refractoriness were determined by RV pacing using a 20-beat drive train (S1, 240 ms cycle length (CL)) followed by an S2 decrementing at 10 ms from 240 ms to 200 ms, and at 5 ms from 200 ms to Effective Refractory Period (ERP); defined as the longest coupling interval that failed to capture the ventricles. Using a custom-written program [11], MAP duration was measured from the beginning of the signal to 90 % repolarization ($MAPD_{90}$) as described previously (Supplementary Fig. 2) [10]. A best-fitted exponential curve was calculated ($MAPD_{90} = MAPD_{90max}\ [1\text{-}e^{-DI/T}]$) and fitted using Microcal Origin (v9.1, Origin, San Diego, CA, US) where T was the time constant. Analysis of the first derivative of this fitted curve yielded the maximum slope of action potential duration restitution (APDR) [12].

The degree of apico-basal APDR dispersion was calculated using the following formula:-.

$$\text{Apico}-\text{basal APDR Dispersion} = [(\text{Apical APDR} - \text{Basal APDR})/\text{Basal APDR}] \times 100\%$$

2.7. Transthoracic echocardiography

Six weeks following surgery, we performed transthoracic echocardiography (TTE) on sedated rabbits (Cohort 1: HF, $n = 13$; SHM, $n = 12$) at the left lateral position to measure both functional and quantitative parameters.

2.8. Ex-vivo cardiac magnetic resonance imaging

Post-experiment whole hearts (Cohort 1, $n = 17$; 10:HF, 7:SHM) were fixed overnight (4 % PFA,0.01 M PB, pH 7.4) before being placed into Fomblin-Y (Sigma Aldrich, UK). Cardiac magnetic resonance (CMR) scans were performed using a 9.4 T Agilent scanner (Agilent Technologies, Santa Clare, CA, USA). Radiofrequency transmission and reception were achieved with a 40 mm millipede transmit/receive RF coil. Hearts were located with fast gradient echo scan. 3D gradient echo

shimming of first and second order shims were performed, and quality was confirmed using point resolved spectroscopy (PRESS) of the water peak.

Different MRI images were generated by variation of radiofrequency pulses applied and collected. T2-weighted images were acquired using a fast spin echo (FSE) sequence with Repetition Time(TR)/Time to Echo (TE) =3000/40 ms, 30 × 30mm field of view (256 × 256 matrix), 36 × 1 mm coronal slices and 3 signal averages (scan duration = 9 mins 42 s). Whereby TR is the amount of time between successive pulse sequences applied to the same slice, and TE represents the time between the delivery of the radiofrequency pulse and the receipt of the echo signal. The resultant images were used to generate 2D slice montage representations of each heart (Fig. 1). For accurate quantification of scar volume, T1-weighted images were acquired using a 3-dimensional magnetization prepared rapid gradient-echo (MP-RAGE) sequence with TR/TE = 6.5/3.3 ms, 40x30x30mm field of view (256 × 192 × 192 matrix) and 2 signal averages (scan duration = 57 mins 39 s). Scar volume was calculated using manual region of interest (ROI) analysis in 3D Slicer (http://www.slicer.org).

2.9. Histological analysis (Cohort 2)

In Cohort 2, twenty-two animals were used for histological examination of ICNS (2.2–4.0 kg) (Supplementary Fig. 1). Animals were assigned to three groups: 1) control (CTL) where no surgery was performed prior to terminal experiment ($n = 11$), 2) HF ($n = 7$) and 3) SHM ($n = 4$). Animals were premedicated as described previously and sacrificed with an overdose of pentobarbitone sodium (Pentoject, 111 ml/kg, Animalcare Ltd., UK) containing heparin (1000 IU, Multiparin, UK). Following bilateral thoracotomy, hearts were perfused with ice-cold phosphate-buffered saline (PBS; 0.01 M, pH 7.4), pressure-inflated in situ, removed from the chest and prefixed then incubated in a hyaluronidase solution as detailed previously (24).

2.10. Histological staining procedure

Pre-fixed hearts were stained using a modified medium (4 h, 4 °C, pH 5.6) containing (in mM): Sodium Acetate 60.0, Acetylthiocholine Iodide 2.0, Sodium Citrate 15.0, $CuSO_4$ 3.0, $K_3Fe(CN)_6$ 0.5, isoOMPA 0.5, along with Triton-X 1 % and Hyaluronidase 0.5 mg/100 ml [13]. Following staining, whole hearts were post-fixed for long-term storage (Paraformaldehyde (PFA), 4 %).

2.11. Whole-mount preparations

Neural structures were visualised from flattened atrial tissue prepared from pressure distended whole hearts [14].Whole hearts were illuminated by a fibre optic light guide system (KL1500 LCD, Schott UK) and imaged using a Leica M80 microscope (Leica Microsystems, Germany) at magnifications between ×0.75–6.

The walls of the atria and interatrial septum were separated from the ventricles along the atrioventricular groove and dissected into distinct regions:-

1. The heart hilum
2. The wall of the conus arteriosus(CA) and left ventricle (LV)
3. The region ventral to the roots of the pulmonary veins(PVs)
4. The root of the right cranial vein (RCV)

Wholemount preparations were pinned flat and dehydrated through a series of graded ethanol solutions (70 %, 90 % and 100 %). Sections were immersed in xylene (Fisher, UK) (30 mins to 2 h) and mounted using Histomount mounting medium (National Diagnostics, UK) and covered with a coverslip for microscopic analysis.

2.12. Microscopic examination and quantitative analysis

Histologically stained neural structures were visualised and imaged using an upright microscope (Axioscope Imager.Z2, Carl Zeiss Ltd., UK). Images were captured using a digital camera (AxioCam, Carl Zeiss Ltd., UK). Overall topography was constructed offline and image examination and analysis was completed using ZEN software (Carl Zeiss Ltd., UK) and Image J 1.49v software. For counting and identifying, neuronal cell bodies and their areas were systematically scanned over the whole mount. The size of clearly visible neuronal somata was measured on digital images using Image J software and expressed as area.

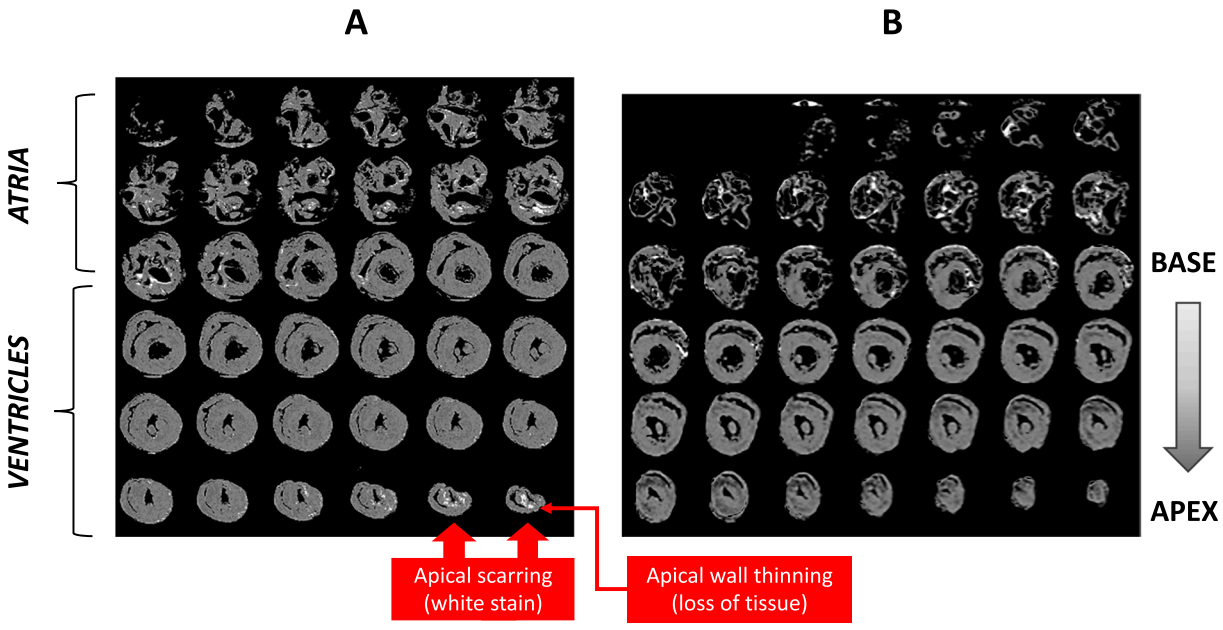

Fig. 1. Examples of ex-vivo T2-weighted 2D slice montage representations (top panels: base; bottom panels; apex) of rabbit heart eight weeks following coronary ligation (1A) with apical scarring (white stain) and wall thinning (loss of tissue)($n = 1$ from group of 10 heart failure rabbits), versus eight weeks following sham procedure (1B) with no evidence of apical scarring ($n = 1$ from group of 7 sham rabbits).

2.13. Statistical analysis

Data analysis was performed using Origin Lab software (v.2015; OriginLab, Northampton, MA, USA) and GraphPad Prism7 software (v7, GraphPad, CA, USA). Statistical comparisons were made using Student's paired *t*-tests, 1- or 2-way ANOVA where appropriate, with Bonferroni post-hoc test. Data are verified to be normally distributed and presented as mean ± SEM; $P \leq 0.05$ being considered significant.

3. Results

Prior to autonomic stimulation, baseline haemodynamics and heart rate (HR) were comparable between HF and SHM groups (Supplementary Table 1).

3.1. Effect of autonomic stimulation on ventricular electrophysiology

3.1.1. VFT

At baseline, VFT in HF group was significantly lower than that in SHM group (HF: 2.5 ± 0.3 mA vs. SHM: 4.0 ± 0.3 mA; $P < 0.05$). Under SNS which increased HR of each group to ~250 bpm, VFT was lower (HF:0.6 ± 0.1 mA; SHM:1.9 ± 0.1 mA; $P < 0.05$). In contrast, VNS led to higher VFT in both HF (3.5 ± 0.4 mA) and SHM (6.8 ± 0.6 mA) with the effect of VNS on VFT attenuated in the HF group (Fig. 2A). Fig. 2B illustrates relative change from the corresponding baseline VFTs in both HF and SHM groups.

The stimulation frequency of both SNS and VNS in the HF and SHM groups were similar in these experiments. To attain a HR of ~250 bpm, the required frequencies of SNS were 8.7 ± 0.1 Hz (HF) and 7.8 ± 1.3 Hz (SHM) respectively. The frequencies of VNS required to achieve a HR of ~60–70 bpm were 10.5 ± 1.4 Hz (HF) and 7.8 ± 0.7 Hz (SHM) respectively.

3.1.2. APD Restitution

APD Restitution (APDR) was assessed by measuring APD90 during an extrastimulus pacing protocol, and by measuring the steepest gradient of the restitution slope (∇) when APD90 was plotted against its preceding diastolic interval (DI). At baseline, the basal LV APDR slope was 2.18 ± 0.07 in HF group whilst basal APDR curve was flatter in SHM with maximum slope at 1.32 ± 0.06. In comparison to basal APDR, APDR at the non-scarring apex of the hearts (referred from here onwards as apical RT) was steeper in both groups (HF: 2.61 ± 0.08, $P = 0.076$; SHM: 1.51 ± 0.06, $P = 0.037$)(Fig. 3A).

SNS steepened both basal and apical APDR curves. In HF group, basal and apical APDR slopes were higher at 3.90 ± 0.10 and 5.12 ± 0.09 respectively. In SHM group, the increase in basal and apical APDR slopes was 2.10 ± 0.09 and 2.58 ± 0.08 correspondingly (Fig. 3A).

VNS flattened both basal and apical APDR curves. Basal and apical APDR slopes in HF groups were 1.48 ± 0.07 and 1.70 ± 0.11. In SHM group, the VNS effect on both basal and apical APDR was significantly more prominent, resulting in lower APDR slope (base:0.61 ± 0.05; apex:0.65 ± 0.06) than those of HF group (Fig. 3A).

Fig. 3B illustrates relative changes in APDR by SNS and VNS from the baseline APDRs. Fig. 3C illustrates typical examples of APDR curves in SHM and HF hearts at baseline, and during SNS and VNS.

3.1.3. Apico-basal restitution dispersion

In this study, apical APDR slopes were steeper than basal APDR in both HF (2.61 ± 0.08 vs. 2.18 ± 0.07, $P \leq 0.001$) and SHM (1.51 ± 0.06 vs. 1.32 ± 0.06, $P = 0.037$) groups. To assess the degree of apico-basal APDR dispersion, the following formula was used:-

$$\text{Apico}-\text{basal APDR Dispersion} = [(\text{Apical APDR} - \text{Basal APDR})/\text{Basal APDR}] \times 100\%$$

In the absence of autonomic stimulation, apico-basal APDR dispersion was greater in HF group (23.7 ± 1.4 %) than that in SHM group (16.8 ± 1.0 %). SNS increased APDR dispersion with its effect augmented in the HF group (HF: 33.0 ± 2.5 % vs. SHM: 25.0 ± 1.8 %). The effect of VNS on dispersion was insignificant compared to baseline. Nonetheless, dispersion of apico-basal APDR remains greater in the HF group (HF: 21.0 ± 2.4 % vs. SHM: 12.4 ± 2.6 %)(Fig. 3D).

3.1.4. Ventricular refractoriness

At baseline, mean ventricular ERP was similar in both groups (HF: 125.9 ± 4.8 ms vs. SHM: 128.8 ± 5.9 ms, $P = 0.666$). During SNS, ERP was shortened (HF: 97.7 ± 2.5 ms vs. SHM: 115.8 ± 3.9 ms, $P = 0.007$). Conversely, VNS produced ERP prolongation, increasing the ventricular ERP to 132.3 ± 4.1 ms (HF) and 150.8 ± 5.3 ms (SHM)(HF vs SHM, $P = 0.006$).

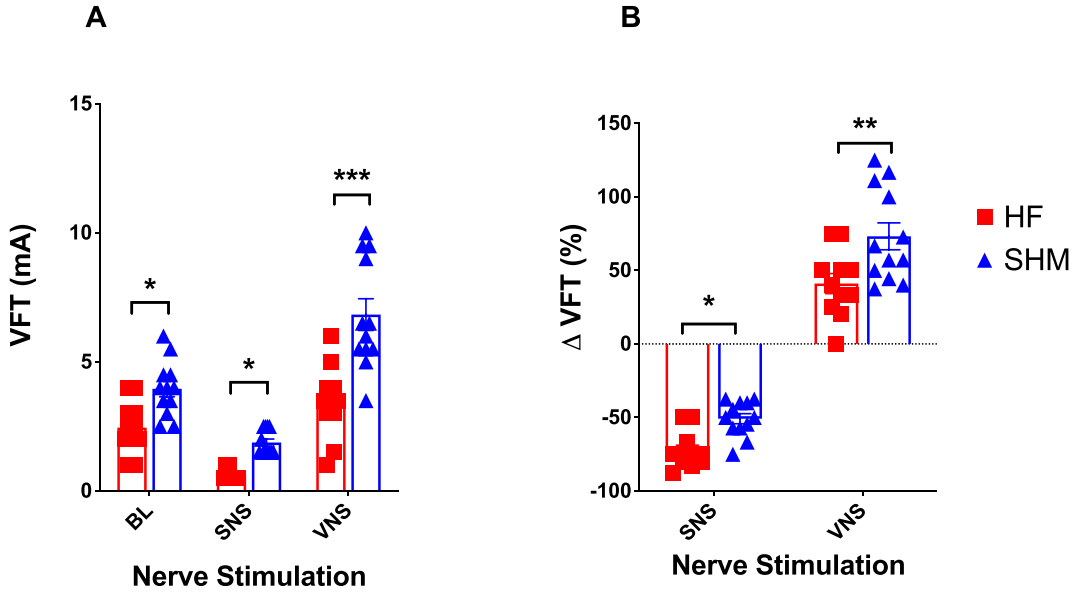

Fig. 2. Comparison of ventricular fibrillation threshold (A) and relative changes from baseline (B) between heart failure (HF)($n = 13$) and sham (SHM)($n = 12$) groups at baseline (BL), during sympathetic (SNS) and vagal (VNS) stimulations with each condition replicated 3 times. Data analyzed as repeated measures 2-way ANOVA with Bonferroni post-hoc test and presented as mean ± SEM; *$p < 0.05$, **$p < 0.01$, ***$p < 0.001$.

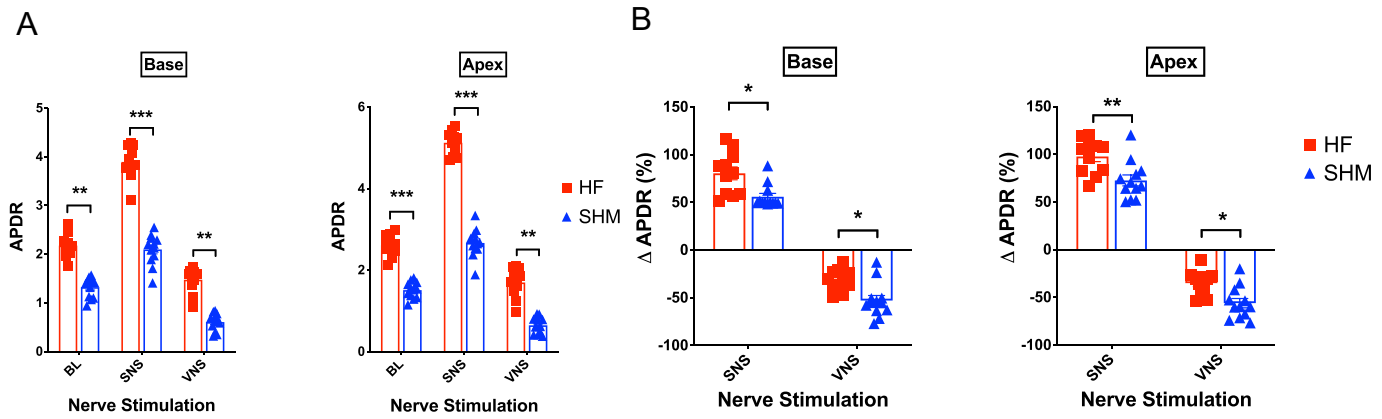

Fig. 3. A Comparison of basal and apical action potential duration-restitution (APDR) between heart failure (HF)($n = 13$) and sham (SHM)($n = 12$) groups at baseline (BL), during sympathetic (SNS) and vagal (VNS) stimulations with each condition replicated 3 times. Data analyzed as repeated measures 2-way ANOVA with Bonferroni post-hoc test and presented as mean ± SEM; $^{*}p < 0.05$, $^{**}p < 0.01$, $^{***}p < 0.001$

B Comparison of relative changes from baseline values in basal and apical action potential duration-restitution (APDR) between heart failure (HF)($n = 13$) and sham (SHM)($n = 12$) groups during sympathetic (SNS) and vagal (VNS) stimulations with each condition replicated 3 times. Data analyzed as repeated measures 2-way ANOVA with Bonferroni post-hoc test and presented as mean ± SEM; $^{*}p < 0.05$, $^{**}p < 0.01$, $^{***}p < 0.001$

C Typical examples of regional restitution (APDR) curves between a heart failure (HF) and sham (SHM) at baseline (3 C*i-ii*), during SNS (*iii-iv*) and VNS (*v-vi*) with each condition replicated 3 times. APDR curves at base (left panel) and apex (right panel) of SHM and HF hearts were shown (n = 1 from group of 13 HF rabbits, and n = 1 from group of 12 SHM rabbits).

D Comparison of relative apico-basal restitution (APDR) dispersion between heart failure (HF) ($n = 13$) and sham (SHM) ($n = 12$) groups. Data analyzed as repeated measures 2-way ANOVA with Bonferroni post-hoc test and presented as mean ± SEM; $^{*}p < 0.05$, $^{**}p < 0.01$, $^{***}p < 0.001$.

SNS exerted a greater effect in ERP shortening in the HF group (HF: −21.7 ± 2.3 % vs. SHM: −9.3 ± 2.5 %, $P < 0.05$). Meanwhile, VNS resulted in ERP prolongation although this effect was attenuated in the HF group (HF: 5.4 ± 1.1 % vs. SHM: 17.9 ± 2.3 %, $P < 0.05$).

3.2. Anatomy and morphology of the rabbit ICNS in heart failure

3.2.1. Quantification of rabbit intrinsic cardiac ganglia in heart failure

A breakdown of the distribution of intrinsic cardiac neurons within distinct regions of the rabbit heart is detailed in Supplementary Table 2. The number of neuronal somata is comparable between CTL and SHM groups (CTL: 1632 ± 216 vs. SHM: 1760 ± 133). In contrast, the average number of neuronal somata per heart was significantly lower in the HF group (HF:1159 ± 101, $P < 0.0001$).

Overall, the average cell area (μm^2) in control animals was 601 ± 45, with no significant regional variation. Conversely, in all HF hearts, there was significant neuronal enlargement (Fig. 4A and B, $P < 0.0001$). The degree of neuronal enlargement in the HF group was spatially diverse. The most significant difference in neuronal size was observed within the region of the heart hilum (HF: 1185 ± 31 μm^2 vs CTL: 632 ± 60 μm^2 vs SHM: 652 ± 50 μm^2). In comparison, neuronal somata from the right atrial region of HF hearts showed no significant enlargement (HF: 752 ± 132 μm^2 vs CTL: 567 ± 68 μm^2 vs SHM: 496 ± 32 μm^2 (Fig. 4B).

3.2.2. Distribution of ICNS in the rabbit heart failure model

In all hearts across CTL, SHM and HF groups, neuronal somata were distributed epicardially, primarily on the heart hilum and at the roots of the pulmonary veins. The majority of neurons were found on supra-ventricular tissues, particularly on the venous part of the heart hilum. Intrinsic cardiac ganglia were also identified at the region of the CA at the root of the pulmonary trunk, termed ventricular neurons (Fig. 5). In all hearts, somata existed either grouped into ganglia (defined as ≥3 neurons), as single cells or as pairs of cells (Fig. 5). In all groups examined, a large number of neuronal somata were distributed into two large clusters: the left and right neuronal clusters (LNC and RNC). In general, the RNC was located at the cranial aspect of the interatrial groove, at the anterior region of the root of the RCV and dorsal to the root of the right PV. The location of the LNC was more diverse in comparison but was commonly found dorsal to the roots of the left and middle PVs.

There was no distinct difference in the overall spatial distribution of cardiac nerves, neurons and ganglia among all 3 groups.

3.3. Cardiac remodeling

3.3.1. In vivo TTE assessment

TTE evaluations revealed a significant degree of LV systolic impairment in the HF group as reflected by the lower ejection fraction (EF), as well as reduced fractional shortening and area change (FAC)(Supplementary Table 3). Enlargement of cardiac chambers was evident in the HF group. Thinning of the interventricular septum was observed, accounting for an eccentricity in the septum:posterior wall thickness ratio (Supplementary Table 3).

3.4. Ex-vivo left ventricular scar quantification

Ex-vivo CMR consistently demonstrated the absence of scar in the LV of the sham animals ($n = 7$) (Supplementary Table 4). In the HF group, 8/10 hearts showed quantifiable LV scar (440.56 ± 95.87 mm^3), suggesting that coronary ligation reliably produced measurable myocardial scarring.

4. Discussion

The current study sets out to demonstrate pathological neurocardiac profile in a rabbit model of heart failure with reduced ejection fraction as a consequence of coronary ligation-induced myocardial infarction. Throughout this study, the term “heart failure” therefore implies heart failure with reduced ejection fraction. Electrophysiologic, neuronal and structural remodeling in HF models when compared to SHM and CTL animals are as follow:-

1. Lower baseline VFT with evidence of exaggerated SNS and attenuated VNS effect in ventricular excitability.

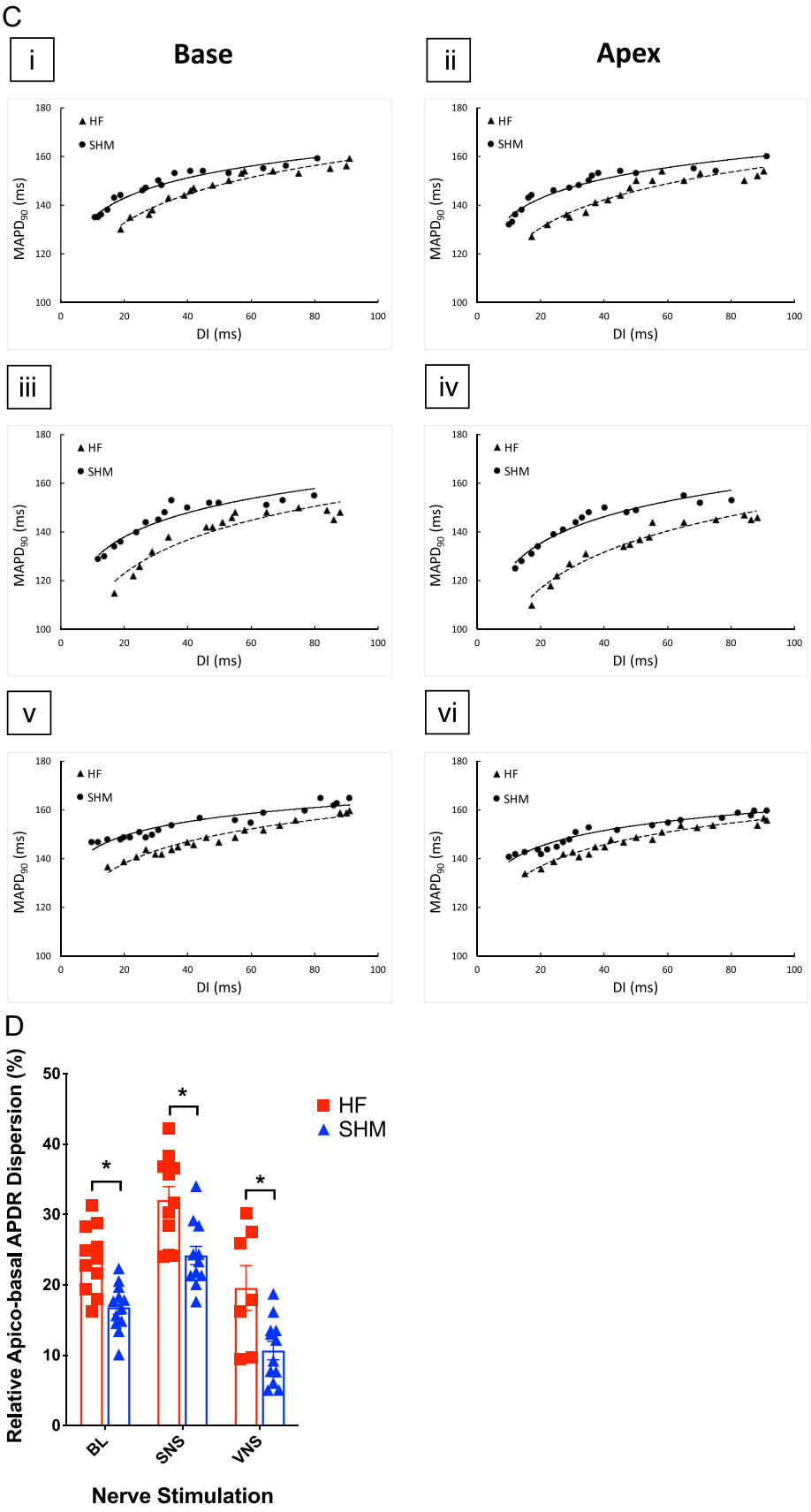

Fig. 3. (*continued*).

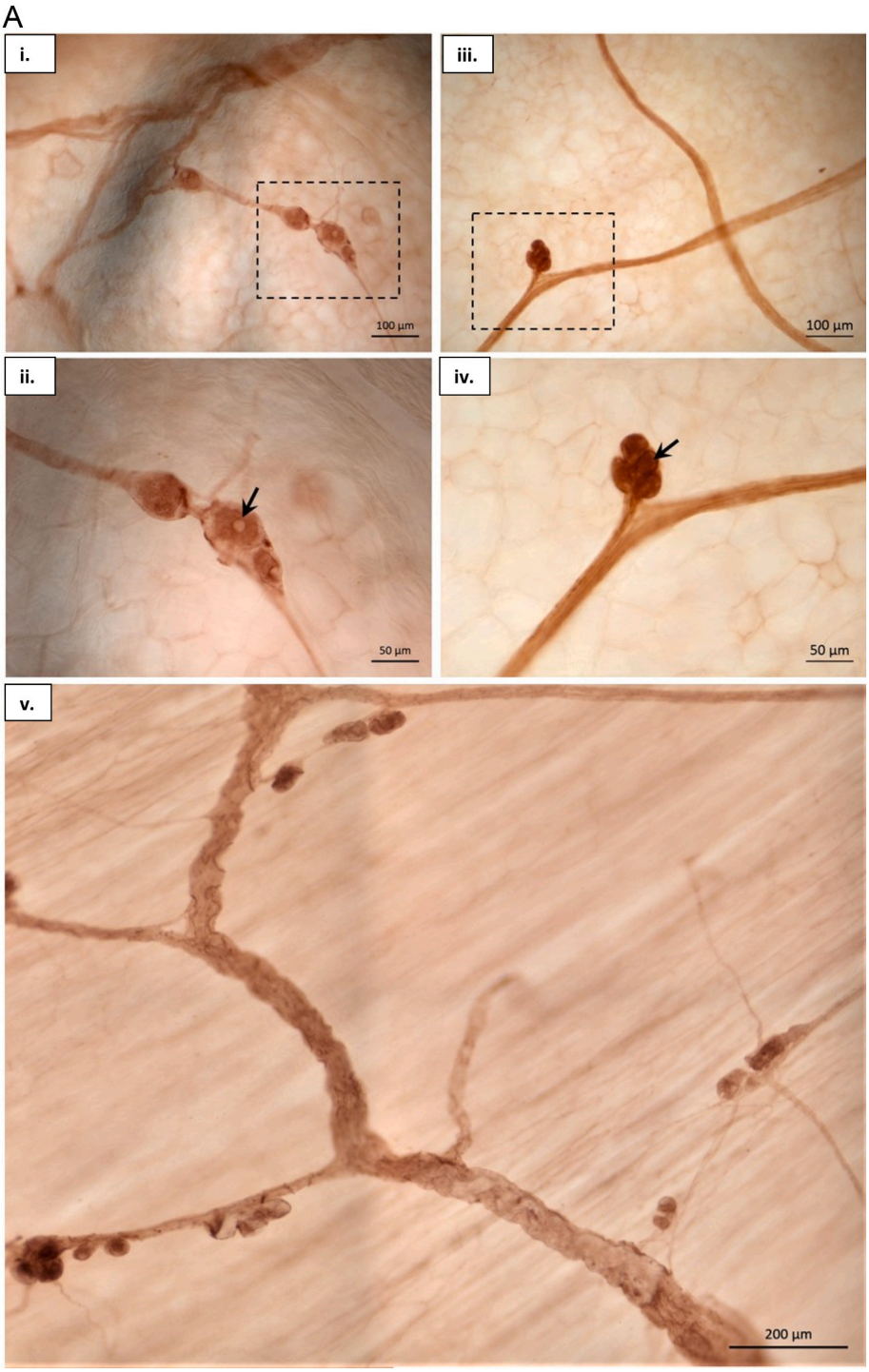

Fig. 4. A Macrographs illustrating the neuronal enlargement of somata seen in the heart failure group (4A*i* and *ii*)($n = 7$) when compared to the control ($n = 11$) group (4A*iii* and *iv*). Micrograph highlighting the lack of neuronal enlargement in the right atrial region in the heart failure group (4A*v*).
B MI induced morphological changes in neuronal somata within the rabbit ICNS. The average overall cell area was quantified and compared between hearts from CTL (green)($n = 11$ (10777), SHM (blue)($n = 4$ (3419) and HF (red)($n = 7$ (3902)) (4B*i*). The average cell area was increased significantly in all regions examined apart from the region of the right atrial ganglionated plexus (4B*ii*). Representations of the distribution of cell size are shown in B*iii*, with B*iv* indicating ganglionic sites and highlighting the right atrial region (red circle). n = number of animals (number of cells). Data are represented as mean ± SEM. Statistical analysis performed with repeated measures two-way ANOVA, with Bonferroni post-hoc test. ns = no significance, $^{***}p < 0.001$, $^{****}p < 0.0001$. Abbreviations: CA, conus arteriosus; RA, right atrial; vPV, ventral pulmonary veins; RCV – right cranial vena cava; LCV – left cranial vena cava; LPV/MPV/RPV – left, middle, right pulmonary vein; DRA/VRA – dorsal/ventral right atrium; VLA – ventral left atrium; RAu – right auricle. (For interpretation of the references to colour in this figure legend, the reader is referred to the web version of this article.)

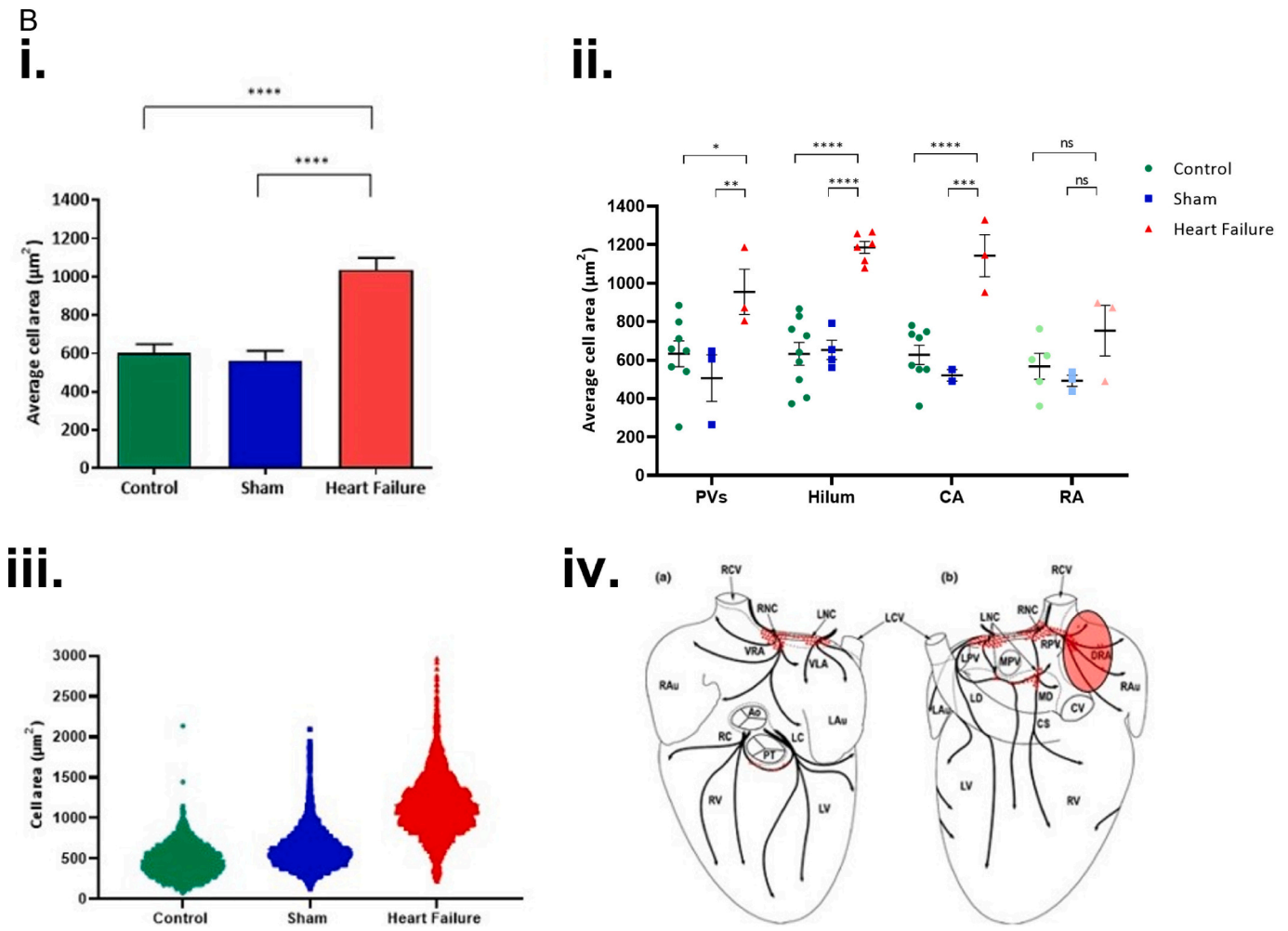

Fig. 4. (*continued*).

2. SNS-exaggeration of shortening in ventricular ERP.
3. Steeper overall APDR with exaggerated SNS steepening and attenuated VNS flattening effects on APDR.
4. Increased apico-basal APDR dispersion in HF animals exaggerated by SNS.
5. Significant neuronal enlargement in HF hearts.
6. No significant difference in distribution of ICNS between HF, SHM and CTL hearts.
7. LV enlargement, wall thinning, myocardial scarring with reduced LV systolic function and in HF animals.

Uniquely, direct autonomic stimulation of isolated, Langendorff rabbit hearts circumvents the confounding effects of perturbed humoral responses and haemodynamic reflexes in other in vivo heart failure studies, allowing the dissection of neurocardiological influences on ventricular electrophysiology. Additionally, it represents a more physiological set up compared to use of exogeneous pharmacological agents in other in vitro heart failure models to simulate sympathetic overdrive and parasympathetic attenuation.

4.1. Autonomic modulation of ventricular electrophysiology in heart failure

This study represents a novel attempt of profiling the effect of autonomic modulation on ventricular electrophysiologic properties in a rabbit heart failure model. Compared to shams, rabbits with heart failure demonstrated an increased arrhythmic susceptibility demonstrable by: 1) lower baseline VFT; 2) exaggerated SNS-induced shortening of ventricular ERP; 3) steeper baseline regional APDR; 4) greater apico-basal APDR dispersion. Underpinning these electrophysiologic remodeling was a deranged autonomic undertone in heart failure rabbits characterized by sympathetic overdrive and vagal attenuation. This is in contrast with the findings of another study in rabbit heart failure model investigating the link between transmural repolarization alternans and VF by optical mapping [15]. Although using identical rabbit heart failure model to assess for ventricular arrhythmic vulnerability, Myles et al. examined fundamentally different ventricular electrophysiologic properties without any autonomic manipulation. Myles et al. concluded that alternans in optical action potential amplitude, but not APD alternans, is associated with VF inducibility by rapid pacing. Discounting the absence of autonomic intervention in Myles' study, several factors may account for the different findings between the current study and the aforementioned study. First, MAP was examined in this study as opposed to optical APD. Second, the current study examined epicardial APD changes on whole-heart preparations as opposed to the wedge preparations used in the other study. Third, the use of mechanical uncoupler in optical mapping studies may influence electrophysiologic properties [16]. Autonomic modulation with SNS and VNS revealed that the pro-arrhythmic effects of SNS were exaggerated in HF whilst the vagal-induced anti-arrhythmic responses were attenuated.

In contrast, vagal protective effect appears to be preserved in a porcine chronic MI model [17]. In particular, there was evidence of preserved acetylcholine levels and parasympathetic neuronal pathway in the infarct border zones with resultant decreasing ventricular

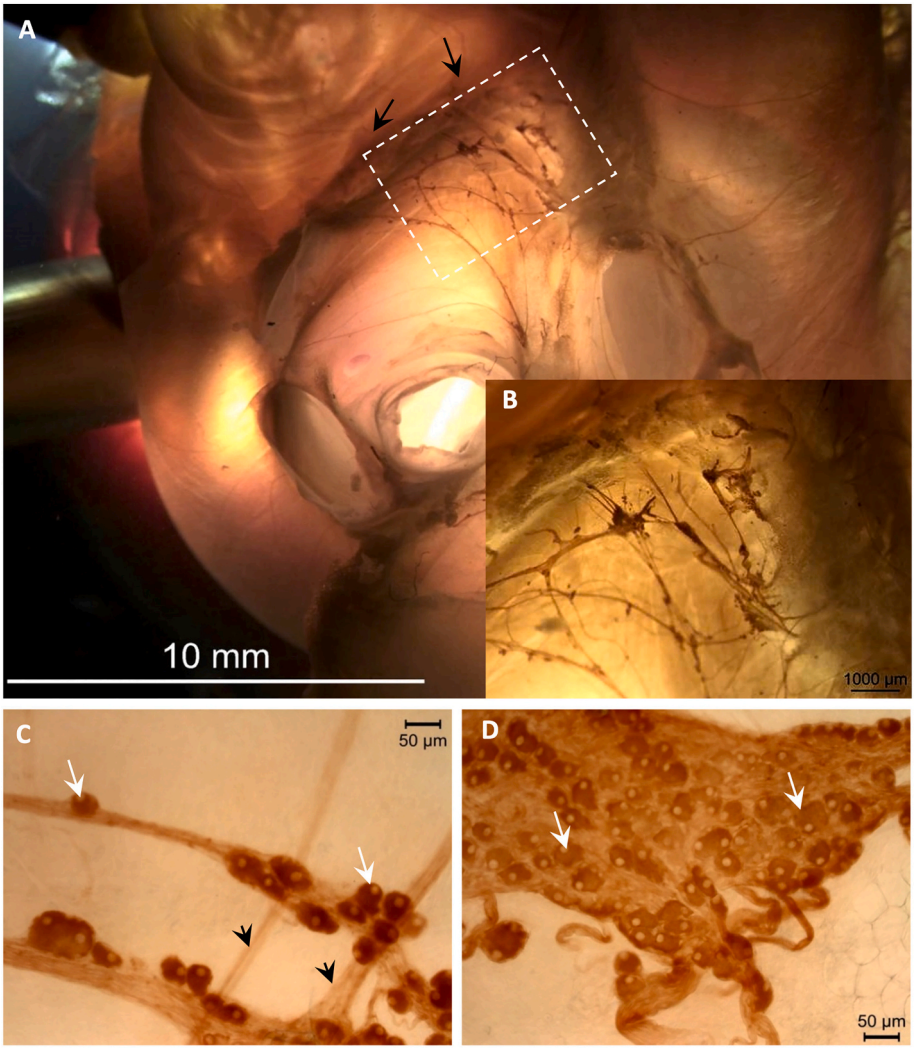

Fig. 5. Macrographs of the rabbit heart illustrating the location of the intrinsic cardiac nerve plexus. The boxed area on the rabbit heart in (a) is enlarged in (b). Images C and D demonstrate examples of right atrial ganglia. Black arrows indicate extrinsic nerves accessing the nerve plexus on the heart hilum in (a) and (b). White arrows indicate examples of intrinsic cardiac neurons with black arrowheads showing interconnecting commissural nerves.

excitability and heterogeneity of repolarization in these areas during VNS. Several explanations are plausible to explain differences in study findings compared to the current study. Aside from species difference in the heart failure models, the timing of the study following the initial MI may play a part with Vaseghi et al. performing the study 6–8 weeks after the MI whereas the current study examined the electrophysiologic response of the heart at least 8 weeks after MI. Of note, VNS protocol was different with Vaseghi et al. performing pulsed VNS (15 s on, 15 s off) as compared to steady-state VNS protocol used in this study. Interestingly in that study, scar borders were defined with conventional bipolar voltages of 0.5–1.5 mV and scars being 0.05–0.5 mV although MRI revealed areas of normal myocardium recording <0.5 mV, supporting the notion of variable (often lower) bipolar voltages in border zones [18]. This may confound the regional electrophysiologic effects of VNS observed in the border zones defined by conventional bipolar voltage definition.

In this study, electrophysiologic remodeling in HF was assessed using single autonomic nerve stimulation. We have previously characterized the effects of sympatho-vagal interaction on ventricular electrophysiology of normal hearts, demonstrating the lack of accentuated antagonism (and therefore prevailing sympathetic effect) at the ventricular level [10]. Instinctively, future studies should assess sympatho-vagal interaction in the in vitro HF model to mimic the complex sympatho-vagal interaction in real life HF population. Furthermore, the effect of downstream stimulation of intrinsic cardiac ganglia will shed further light on electrophysiologic remodeling in HF.

4.2. *Electrical restitution and spatial restitution dispersion in heart failure*

The restitution hypothesis proposed by Weiss et al. postulates that a steep slope of an APDR curve with a gradient of >1 promotes oscillations and wave breaks, ultimately facilitating the initiation of ventricular fibrillation in the myocardium [19]. This hypothesis was validated in biological models [12] as well as pharmacological studies [20,21].

In this study, baseline standard restitution slopes measured at the LV base were > 1 (i.e., 1.32 ± 0.06 SHM vs. 2.18 ± 0.07 HF). This is in line with restitution slope values in a normal unstimulated in vitro model of rabbit hearts [22]. Although Weiss et al. proposed a gradient of >1 with arrhythmic vulnerability, this hypothesis is borne out of a mathematical model. A more realistic and valid comparison of baseline APDR should be based on previous unstimulated normal rabbit hearts [22]. More importantly, in unstimulated hearts at baseline, HF group demonstrated a steeper restitution slope than SHM group.

Furthermore, this study demonstrated regional heterogeneity in restitution slopes between the basal and apical regions of the LV epicardium in rabbits. In general, apical restitution slopes are steeper

than the restitution slopes at base in both groups. This is likely to be accountable by the RV apical pacing site in close proximity to the LV apex [23]. Nonetheless, the degree of dispersion overall remains greater in the HF group, suggesting increased spatial electrical heterogeneity (Fig. 3D). The steeper apical restitution persisted during SNS despite well-demonstrated greater SNS innervation basally in mammalian hearts [24,25]. This phenomenon is accountable by differential functional innervation in the apical region. Heightened sensitivity to noradrenaline infusion attributable to increased adrenoreceptors in this region compensates for the relatively sparse sympathetic distribution [26]. This is further supported by our previous study demonstrating not only increased dispersion but also change in repolarization by SNS in isolated rabbit hearts [27].Indeed, bilateral VNS and SNS have respectively been shown to reverse dispersion of repolarization from base to apex in that study. In contrast, crude directional APDR changes was absent in the current study. In a porcine infarct model, Dries et al. demonstrated a higher incidence of delayed after-depolarizations and beat-to-beat variability of repolarization in the peri-infarct zone but not the remote regions of the infarct heart during isoprenaline infusion [28]. We have not examined this phenomenon, but assessment of these parameters will provide further insight in the current model during intrinsic autonomic nerve stimulation in future studies.

4.3. Autonomic modulation of electrical restitution and ventricular refractoriness in heart failure

The effect of autonomic modulation on electrical restitution and ventricular refractoriness in normal hearts is well known [29]. Adrenergic stimulation by either direct SNS or adrenergic agonists, causes a downward shift in APDR curve in addition to steepening the restitution slope in both in vivo [30] and in vitro [22] animal studies as well as clinical studies [21]. In addition, the shorter APD during SNS is associated with ERP shortening in both in vivo [31] and in vitro studies [22]. All these studies validated the sympathetic effects observed in this study. In both SHM and HF groups, SNS resulted in steepening of both basal and apical restitution slopes in addition to shortening ventricular ERP. Notably, these sympathetic-driven effects on ventricular electrophysiology are more evident in the HF group (Fig. 3A, B). Furthermore, there was an increased apico-basal restitution dispersion (Fig. 3D) with greater dispersion seen in the HF group, corroborating previous study demonstrating increased dispersion of repolarization in rabbit hearts during SNS [27], thereby producing an arrhythmogenic effect on a whole-heart level in addition to the well-described adrenergic effect on abnormal calcium handling in HF at a cellular level [32].

In contrast, VNS produced an upward shift of the APDR curve with associated flattening of the restitution slope. Additionally, ventricular ERP was prolonged by VNS in congruent with its effect on APD prolongation in in vivo [31] and in vitro studies [22]. In this study, similar phenomena were observed but in the HF group, the ERP was shorter and restitution slopes were steeper when compared to the shams, suggesting an attenuated vagal effect in HF. Spatial heterogeneity in apico-basal restitution kinetics was unaltered during vagal stimulation compared to baseline in both shams and HF groups. The effect of vagal stimulation on dispersion of repolarization has been debatable. Although one study demonstrated greater spatial dispersion of repolarization in the context of vagal bradycardia and APD prolongation [33], the findings in this study is in agreement with another study demonstrating unaltered magnitude of dispersion of repolarization in rabbit hearts [27].

4.4. Neural remodeling in heart failure

This study is the first study to detail the gross neuroanatomy and morphological remodeling of the ICNS in the chronically infarcted rabbit heart, unlike previous studies where hypertrophy and remodeling was documented in isolated cardiac regions only [5,34,35]. This is also the first study to highlight reduced neuronal numbers within the ICNS in cardiac disease. The morphological pattern of the ICNS was concentrated within the heart hilum, in agreement with earlier investigations in mice, rabbits, dogs and sheep [36].

To date, current information regarding neuronal remodeling within the ICNS in response to MI is limited. The results indicate differentially targeted neuronal enlargement within the rabbit ICNS following MI. This data would appear to strengthen the conclusions of recent porcine studies that MI induces morphological changes in ganglia, the latter of which exert preferential influence over the infarcted ventricles [34].

Of particular interest is the reduction in cell number seen in HF. Such neuronal reduction may correlate with a decrease in cholinergic neurons within the ICNS following MI [34] and contribute to central vagal attenuation, with further characterization of the immunohistochemical profile of the rabbit atrial epicardial network following MI being needed to identify the complex mechanisms underlying remodeling and hypertrophy. The apparent lack of neuronal remodeling within the right atrial ganglionic plexus, a region dominant in the control of heart rate [37], is likely to be due to the fact that this ganglia preferentially exerts influence over the atria [38] and is therefore somewhat isolated and protected from neural supply to the site of injury. Future studies with bigger sample size and detailed neuronal phenotyping will provide validation of these findings in addition to more intricate details on neuronal remodeling.

Evidence shows that neural innervation of the ventricles originates from numerous ganglia located both 1) at the level of the ventricles and on the CA and 2) atrially, at the venous portion of the heart hilum and roots of the PVs [14,39]. Adaptations within such regions, accompanied by neurophenotypic alterations and changes in the functional capacity within the ICNS [34] therefore suggests an involvement of the ICNS in providing a certain level of protection against the central neuronal dysregulation during MI.

4.5. Cardiac remodeling in heart failure

TTE and CMR data in this study provides valuable insights in both regional and global ventricular function in the rabbit HF model following coronary ligation. The decreased septal thickness in comparison to posterior wall thickness in the HF group provides relative evidence of regional wall motion abnormality induced by apical infarct (Supplementary Table 3). Furthermore, the increased end-diastolic volume and endocardial area signifies increased LV radius, producing a change in ventricular geometry in which the heart assumes a more spherical shape [40].

Myocardial scarring, as demonstrated by CMR in this study, causes impairment of myocardial contractility, thereby leading to reduced stroke volume and EF on TTE. This relationship between myocardial scar on MRI and LV systolic function on TTE is in parallel with that in humans [41], providing valuable insights in establishing the structure-function relationship in current HF model.

4.6. Limitations

The current in vitro rabbit heart failure model with isolated autonomic stimulation has several limitations. Given the in vitro set up, there is no central input and therefore the effect of afferent VNS was not examined. Although SNS was achieved through spinal cord stimulation, it should be acknowledged that this is not isolated SNS, the latter of which could be assessed by stellate ganglia stimulation in future studies [42]. Male rabbits were used in this study for consistency in data comparison with historical normal heart studies within the group. The use of female rabbits would allow for assessment of additional hormonal effects on autonomic modulation of ventricular electrophysiology, but this is beyond the scope of the current study. Although previous in vitro study from our group demonstrated increased propensity of alternans with dynamic pacing over a greater range of pacing cycle lengths during SNS [22], only standard restitution was assessed in this study with no dynamic pacing protocol to assess alternans response.

5. Conclusion

In a rabbit HF model induced by MI following coronary ligation, extensive neuronal and structural remodeling occurs, leading to an adverse electrophysiological profile during autonomic modulation, thereby underpinning key mechanisms in driving dysautonomia-associated ventricular arrhythmias. Future autonomic studies could include optical mapping to investigate regional electrophysiologic heterogeneity but the limitations of the need for mechanical uncouplers which may exert direct electrophysiological effects on repolarisation and APD restitution [11,16] would need to be considered.

Supplementary data to this article can be found online at https://doi.org/10.1016/j.jmccpl.2023.100044.

Funding

This work was supported by a British Heart Foundation Clinical Research Fellowship [FS/12/52/29629 to S. H. C] and a British Heart Foundation Programme Grant (RG/17/3/32774).

Declaration of competing interest

The authors declare the following financial interests/personal relationships which may be considered as potential competing interests: Shui Hao Chin reports financial support was provided by British Heart Foundation. Andre Ng reports financial support was provided by British Heart Foundation.

References

[1] Schwartz PJ, Vanoli E, Stramba-Badiale M, De Ferrari GM, Billman GE, Foreman RD. Autonomic mechanisms and sudden death. New insights from analysis of baroreceptor reflexes in conscious dogs with and without a myocardial infarction. Circulation 1988;78(4):969–79.
[2] Nolan J, Batin PD, Andrews R, Lindsay SJ, Brooksby P, Mullen M, et al. Prospective study of heart rate variability and mortality in chronic heart failure: results of the United Kingdom heart failure evaluation and assessment of risk trial (UK-heart). Circulation 1998;98(15):1510–6.
[3] W. E, B. K. Characterization of the intrinsic cardiac nervous system Autonomic neuroscience: basic & clinical 2016;199:3–16.
[4] Ardell JL, Armour JA. Neurocardiology: structure-based function. Compr Physiol 2016;6(4):1635–53.
[5] Nakamura K, Ajijola OA, Aliotta E, Armour JA, Ardell JL, Shivkumar K. Pathological effects of chronic myocardial infarction on peripheral neurons mediating cardiac neurotransmission. Auton Neurosci 2016;197:34–40.
[6] S. Institute of Medicine Committee on Understanding the Biology of, D. Gender. The National Academies collection: reports funded by National Institutes of Health. In: Wizemann TM, Pardue ML, editors. Exploring the Biological Contributions to Human Health: Does Sex Matter? US: National Academies Press; 2001. Copyright 2001 By the National Academy of Sciences. All rights reserved., Washington (DC).
[8] Ng GA, Brack KE, Coote JH. Effects of direct sympathetic and vagus nerve stimulation on the physiology of the whole heart–a novel model of isolated Langendorff perfused rabbit heart with intact dual autonomic innervation. Exp Physiol 2001;86(3):319–29.
[9] Carnel SB, Schraeder PL, Lathers CM. Effect of phenobarbital pretreatment on cardiac neural discharge and pentylenetetrazol-induced epileptogenic activity in the cat. Pharmacology 1985;30(4):225–40.
[10] Chin SH, Allen E, Brack KE, Ng GA. Effects of sympatho-vagal interaction on ventricular electrophysiology and their modulation during beta-blockade. J Mol Cell Cardiol 2020;139:201–12.
[11] Kettlewell S, Walker NL, Cobbe SM, Burton FL, Smith GL. The electrophysiological and mechanical effects of 2,3-butane-dione monoxime and cytochalasin-D in the Langendorff perfused rabbit heart. Exp Physiol 2004;89(2):163–72.
[12] Cao JM, Qu Z, Kim YH, Wu TJ, Garfinkel A, Weiss JN, et al. Spatiotemporal heterogeneity in the induction of ventricular fibrillation by rapid pacing: importance of cardiac restitution properties. Circ Res 1999;84(11):1318–31.
[13] Pauza DH, Skripka V, Pauziene N, Stropus R. Anatomical study of the neural ganglionated plexus in the canine right atrium: implications for selective denervation and electrophysiology of the sinoatrial node in dog. Anat Rec 1999;225(3):271–94.
[14] Saburkina I, Gukauskiene L, Rysevaite K, Brack KE, Pauza AG, Pauziene N, et al. Morphological pattern of intrinsic nerve plexus distributed on the rabbit heart and interatrial septum. J Anat 2014;224(5):583–93.
[15] Myles RC, Burton FL, Cobbe SM, Smith GL. Alternans of action potential duration and amplitude in rabbits with left ventricular dysfunction following myocardial infarction. J Mol Cell Cardiol 2011;50(3):510–21.
[16] Brack KE, Narang R, Winter J, Ng GA. The mechanical uncoupler blebbistatin is associated with significant electrophysiological effects in the isolated rabbit heart. Exp Physiol 2013;98(5):1009–27.
[17] Vaseghi M, Salavatian S, Rajendran PS, Yagishita D, Woodward WR, Hamon D, et al. Parasympathetic dysfunction and antiarrhythmic effect of vagal nerve stimulation following myocardial infarction. JCI Insight 2017;2(16).
[18] Roca-Luque I, Zaraket F, Garre P, Sanchez-Somonte P, Quinto L, Borras R, et al. Accuracy of standard bipolar amplitude voltage thresholds to identify late potential channels in ventricular tachycardia ablation. J Interv Card Electrophysiol 2023;66(1):15–25.
[19] Weiss JN, Chen PS, Qu Z, Karagueuzian HS, Lin SF, Garfinkel A. Electrical restitution and cardiac fibrillation. J Cardiovasc Electrophysiol 2002;13(3):292–5.
[20] Garfinkel A, Kim YH, Voroshilovsky O, Qu Z, Kil JR, Lee MH, et al. Preventing ventricular fibrillation by flattening cardiac restitution. Proc Natl Acad Sci U S A 2000;97(11):6061–6.
[21] Taggart P, Sutton P, Chalabi Z, Boyett MR, Simon R, Elliott D, et al. Effect of adrenergic stimulation on action potential duration restitution in humans. Circulation 2003;107(2):285–9.
[22] Ng GA, Brack KE, Patel VH, Coote JH. Autonomic modulation of electrical restitution, alternans and ventricular fibrillation initiation in the isolated heart. Cardiovasc Res 2007;73(4):750–60.
[23] Pitruzzello AM, Krassowska W, Idriss SF. Spatial heterogeneity of the restitution portrait in rabbit epicardium. Am J Physiol Heart Circ Physiol 2007;292(3):H1568–78.
[24] Crick SJ, Anderson RH, Ho SY, Sheppard MN. Localisation and quantitation of autonomic innervation in the porcine heart II: endocardium, myocardium and epicardium. J Anat 1999;195(Pt 3):359–73.
[25] Brack KE. The heart's 'little brain' controlling cardiac function in the rabbit. Exp Physiol 2015;100(4):348–53.
[26] Mori H, Ishikawa S, Kojima S, Hayashi J, Watanabe Y, Hoffman JI, et al. Increased responsiveness of left ventricular apical myocardium to adrenergic stimuli. Cardiovasc Res 1993;27(2):192–8.
[27] Mantravadi R, Gabris B, Liu T, Choi BR, de Groat WC, Ng GA, et al. Autonomic nerve stimulation reverses ventricular repolarization sequence in rabbit hearts. Circ Res 2007;100(7):e72–80.
[28] Dries E, Amoni M, Vandenberk B, Johnson DM, Gilbert G, Nagaraju CK, et al. Altered adrenergic response in myocytes bordering a chronic myocardial infarction underlies in vivo triggered activity and repolarization instability. J Physiol 2020;598(14):2875–95.
[29] Ng GA. Neuro-cardiac interaction in malignant ventricular arrhythmia and sudden cardiac death. Auton Neurosci 2016;199:66–79.
[30] Taggart P, Sutton P, Lab M, Dean J, Harrison F. Interplay between adrenaline and interbeat interval on ventricular repolarisation in intact heart in vivo. Cardiovasc Res 1990;24(11):884–95.
[31] Martins JB, Zipes DP. Effects of sympathetic and vagal nerves on recovery properties of the endocardium and epicardium of the canine left ventricle. Circ Res 1980;46(1):100–10.
[32] Johnson DM, Antoons G. Arrhythmogenic mechanisms in heart failure: linking β-adrenergic stimulation, stretch, and calcium. Front Physiol 2018;9:1453.
[33] Yamakawa K, So EL, Rajendran PS, Hoang JD, Makkar N, Mahajan A, et al. Electrophysiological effects of right and left vagal nerve stimulation on the ventricular myocardium. Am J Physiol Heart Circ 2014;307(5):H722–31.
[34] Rajendran PS, Nakamura K, Ajijola OA, Vaseghi M, Armour JA, Ardell JL, et al. Myocardial infarction induces structural and functional remodeling of the intrinsic cardiac nervous system. J Physiol 2016;594(2):321–41.
[35] Hopkins DA, Macdonald SE, Murphy DA, Armour JA. Pathology of intrinsic cardiac neurons from ischemic human hearts. Anat Rec 2000;259(4):424–36.
[36] Saburkina I, Rysevaite K, Pauziene N, Mischke K, Schauerte P, Jalife J, et al. Epicardial neural ganglionated plexus of ovine heart: anatomic basis for experimental cardiac electrophysiology and nerve protective cardiac surgery. Heart Rhythm 2010;7(7):942–50.
[37] Allen E, Coote JH, Grubb BD, Batten TFC, Pauza DH, Ng GA, et al. Electrophysiological effects of nicotinic and electrical stimulation of intrinsic cardiac ganglia in the absence of extrinsic autonomic nerves in the rabbit heart. Heart Rhythm 2018;15(11):1698–707.
[38] Cardinal R, Page P, Vermeulen M, Ardell JL, Armour JA. Spatially divergent cardiac responses to nicotinic stimulation of ganglionated plexus neurons in the canine heart. Auton Neurosci 2009;145(1–2):55–62.
[39] Pauza DH, Skripka V, Pauziene N. Morphology of the intrinsic cardiac nervous system in the dog: a whole-mount study employing histochemical staining with acetylcholinesterase. Cells Tissues Organs 2002;172(4):297–320.
[40] Buckberg GD, Weisfeldt ML, Ballester M, Beyar R, Burkhoff D, Coghlan HC, et al. Left ventricular form and function: scientific priorities and strategic planning for development of new views of disease. Circulation 2004;110(14):e333–6.
[41] A.N.R. Hamrell B.B., Cellular basis of the mechanical properties of hypertrophied myocardium, in: H.E. Fozzard H.A., Jennings R.B., Katz A.M., Morgan H.E. (Ed.), The heart and cardiovascular system, Raven Press, New York (NY), pp. 1507–1524.
[42] Kawashima T. The autonomic nervous system of the human heart with special reference to its origin, course, and peripheral distribution. Anat Embryol (Berl) 2005;209(6):425–38.